Rev. 1
October, 1978

Part I
Chapter 2

Advanced Recycle Methodology Program

System Documentation

Research Project 118-1

EPRI-CELL Criticals Benchmarking

October 30, 1978

Prepared for:

Electric Power Research Institute
3412 Hillview Avenue
Palo Alto, CA 94304

Principal Investigators

W. J. Eich (NAI)*
M. L. Kennedy (NAI)
R. D. Mosteller (Science Applications, Inc.)

EPRI Project Manager

B. A. Zolotar

Prepared by:

Nuclear Associates International Corporation
6003 Executive Boulevard
Rockville, MD 20852

With revisions by:
Electric Power Research Institute

* Current affiliation: Electric Power Research Institute
Palo Alto, CA 94303

TABLE OF CONTENTS

effect, however, adds several tenths of a percent in reactivity to very watery lattices but such are so far from reactor conditions that their analysis lacks most practical relevance.) Finally, the two items of input required for the simulation of grain heterogeneities have been entered for the MO_2 cases.

Box 3 of Figure 2-1 signifies the non-depletion EPRI-CELL (GAM/THERMOS) run which produces printed output (Box 4) and, by option, the few PDQ-7 input cards containing the macroscopic few group EPRI-CELL output in Table Set Format (Box 5). These cards are part of the input to a "one-dimensional" radial plane PDQ-7 - Box 7 (one mesh in the Z-direction with zero current boundaries). Another item of input is the axial buckling, B_z^2, (Box 6) which has generally been measured. If this buckling was not available in the literature, then it has been accurately estimated from measured critical water heights and reflector savings measured in similar lattices. Since the criticals analyzed in the course of this Program have been restricted to arrays having relatively high moderator heights, dependence of the final value of k_{eff} (Box 8) is quite minimal on axial buckling uncertainty. Another item of input to these PDQs is a set of (four fast group) reflector constants which were developed to match the results of multigroup transport (P3) calculations[4]. These critical analyses could as validly have been conducted with 3 fast groups mutatis mutandis[5] but the effort had been initiated before the installation of the collapsed broad group edits. The Mixed Number Density model is implicit in the core and reflector thermal group constants used in these PDQ calculations.

The approach used in analyzing large-scale mock-up experiments differs in some respects from the procedure discussed above. That approach is described in more detail in Section 6 of this Chapter.

SECTION 6

LARGE-SCALE MOCK-UP RESULTS

6.1 Introduction

Figure 6-1 schematically illustrates the calculational process followed in the analysis of five large-scale mock-ups. The procedure is basically similar to the approach described in Section 2 of this chapter for critical lattices. There are three principal differences between the two methodologies:

(1) the large-scale mock-ups were analyzed for the verification of existing ARMP libraries and procedures rather than to aid in the development of the system

(2) the mock-ups were sufficiently heterogeneous that two-dimensional rectangular diffusion theory calculations were required in place of one-dimensional radial calculations

(3) separate EPRI-CELL calculations were required for different parts of lattices--fuel pins, water holes, and burnable poison pins

These mock-ups are of special interest because they permit accurate determination of the worth of burnable poison rods (BPR's). Heretofore, BPR contributions to reactivity in PWR's have been subsumed into core analyses which integrate a number of additional effects, such as control rod worth, Xenon worth, Doppler defect, and soluble boron worth. These mock-ups, however, determine the BPR worth up to 9 percent $\Delta\rho$ by means of straightforward soluble boron substitution. Furthermore, these particular BPR's have a boron loading which is approximately 70 percent heavier than that for PWR assemblies of any current design. The agreement achieved with the experimental data therefore uniquely validates the ARMP representation of burnable poisons and, in addition, further substantiates the benchmarking of EPRI-CELL against critical experiments, which is described in the preceding sections of this chapter.

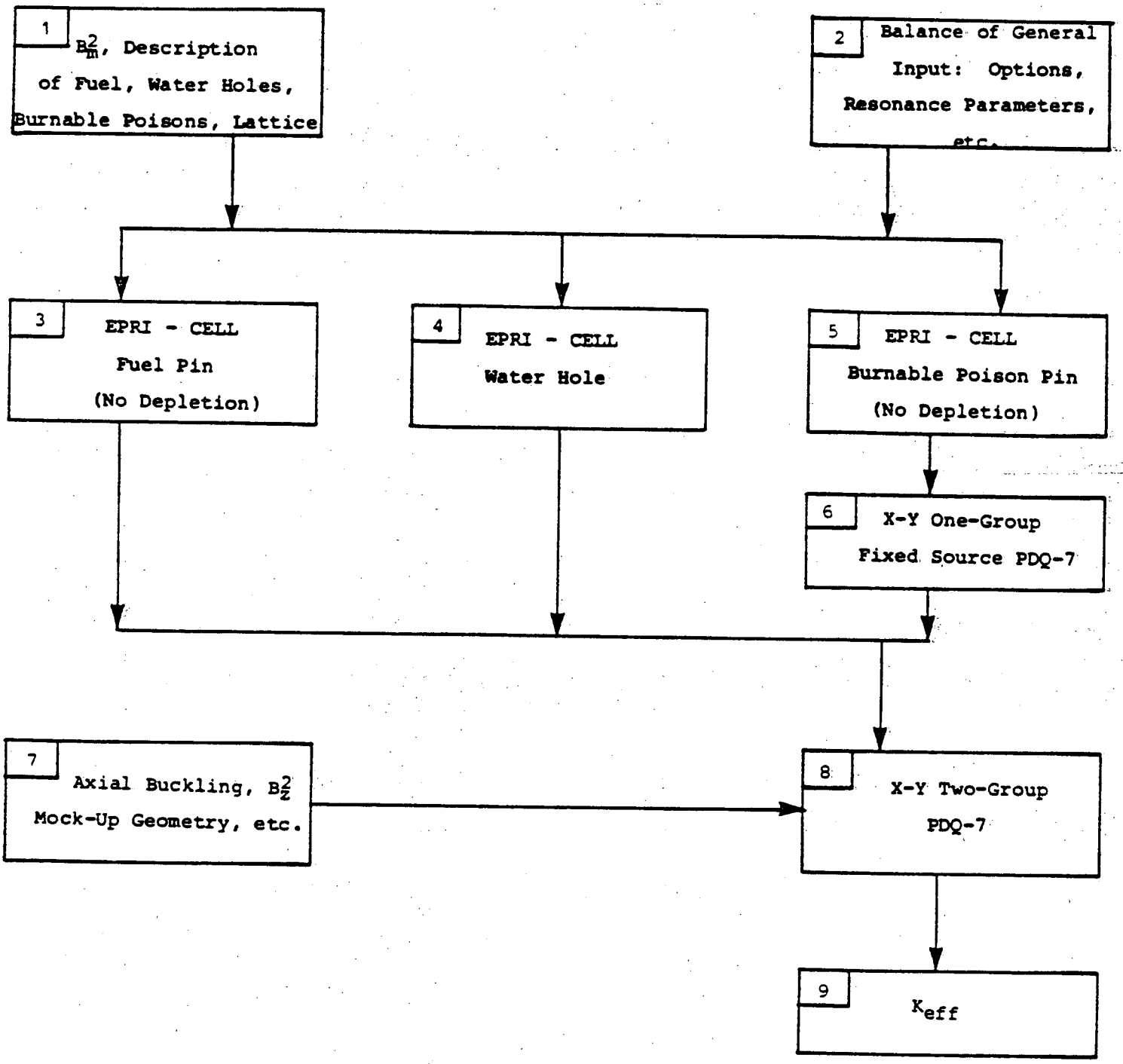

FIGURE 6-1 Flow Chart for Large-Scale Mock-Up Analysis

6.2 Description of Experiments[21]

The experimental configuration employed in these critical mock-ups is shown in Figure 6-2. The subassembly regions indicated there are fictitious in the sense that there is no structural material in the active region of the geometry and that there is no physical significance to the subassembly boundary. A subassembly region, however, does correspond to a 15 x 15 assembly in size and configuration. The outer buffer region was comprised only of fuel pins and borated moderator, but the contents of the subassembly regions were rearranged from case to case and the soluble boron concentration was adjusted until a multiplication factor of 1.0007 was achieved. The subassembly configurations for the different cases, or "loads," are summarized in Figure 6-3. All locations other than those indicated are fuel cells.

The fuel pins and burnable poison rods are described in Table 6-1. Unlike normal fuel pins, these pins are clad with aluminum. The BPR's are unclad cylinders of pyrex glass which have a much higher boron content than normal BPR's. Water holes contain nothing but borated water, and moderator characteristics are summarized in Table 6-1, as well. All measurements were performed at room temperature and pressure, with a moderator height of 145 cm.

For the loadings of interest in this study relative power densities were obtained for one octant of the central subassembly. These measurements were made at the midplane of the active height, using a sodium iodide (thallium activated) scintillation counter to count collimated fission-product gamma rays from activated fuel rods.

The five loadings considered here allow direct determination of BPR worth by the method of soluble boron substitution. In load 1 the subassemblies contain a uniform lattice of fuel pins, and the central region is identical to the buffer. In loads 2 and 3, 17

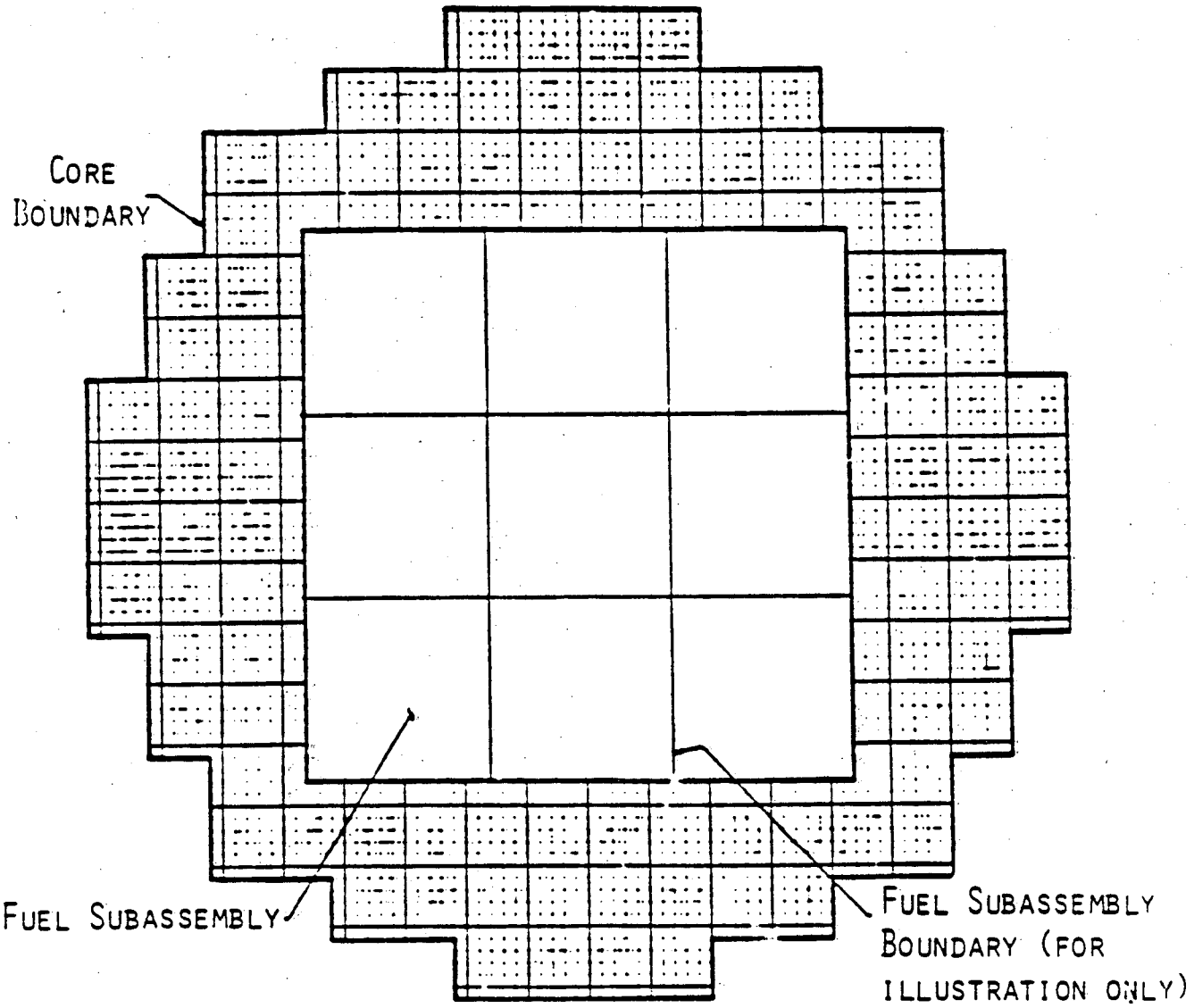

FIGURE 6.2 Geometry for Large-Scale Mock-Up Experiments

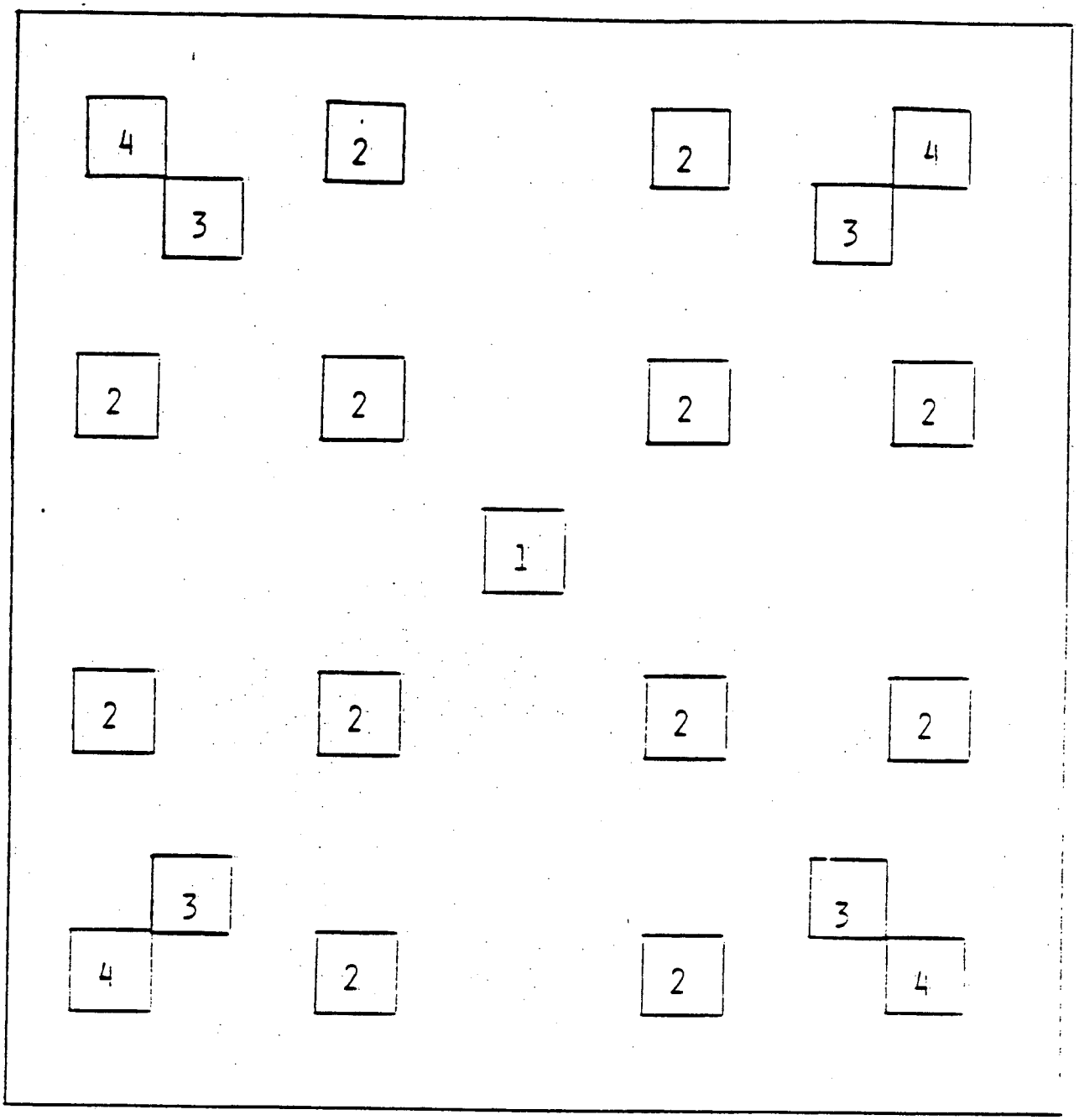

	Load 1	Load 2	Load 3	Load 8	Load 9
Location 1	Fuel	Water	Water	Water	Water
Locations 2	Fuel	Water	Water	Poison	Poison
Locations 3	Fuel	Water	Fuel	Poison	Fuel
Locations 4	Fuel	Fuel	Water	Fuel	Poison

FIGURE 6-3 Subassembly Configurations

TABLE 6-1

PHYSICAL CHARACTERISTICS OF PINS AND MODERATOR

Fuel Pin

Enrichment, w/o	2.459, ± .002
Pellet Material	UO_2
Pellet Density, g/cm^3	10.24 ± .04
Pellet Diameter, cm	1.0297 ± .0013
Active Fuel Length, cm	153.34 ± .89
Clad Material	6061 Aluminum
Clad Thickness, cm	.0813 ± .0025
Clad Outer Diameter, cm	1.2060 ± .0015
Fuel Pin Pitch, cm	1.636 ± .003

Burnable Poison Rod

Poison Material	Pyrex Glass
Poison Density, g/cm^3	2.244 ± .008
Poison Diameter, cm	1.170 ± .001
Boron Content, w/o	3.919 ± .002
Poison Length, cm	188.0 ± .1
Clad	None

Moderator

Water Density, g/cm^3	.9978
Water Temperature, °C	21 ± 1
Soluble Boron Content, ppm	
Load 1	1511 ± 3
Load 2	1335.5 ± 3
Load 3	1335.5 ± 3
Load 8	794 ± 3
Load 9	779 ± 3

fuel pins have been removed from each of the subassemblies, leaving borated water in their place. In both loads the subassemblies are octant symmetric, but the water hole locations are slightly different. In loads 8 and 9 the same fuel pins have been removed as in loads 2 and 3, respectively, but BPR's have been inserted in their place everywhere except in the central location of each subassembly. Comparison of results from loads 2 and 8 and from loads 3 and 9 therefore provides a value for the BPR worth in terms of the change in the soluble boron concentration.

6.3 Analytical Procedure

Loads 1, 2 and 8 first were simulated with the standard ARMP PWR procedures described in Part I, Chapter 6 of this documentation, following the process indicated in Figure 6-1. It is to be emphasized that only the standard procedures were used -- more detailed treatments normally employed during benchmarking against critical experiments, such as four energy groups and four mesh spaces per pin cell side in the two-dimensional PDQ calculation, were not needed because of the very low leakage of all these configurations.

This approach produces very good agreement with the experimental data for loads 1 and 8 but not as good for load 2. In the ARMP procedure, a four-group fine-mesh correction is applied to the multiplication factor when water holes are present (see Part I, Chapter 8, Section B), but the discrepancy in the result for load 2 is somewhat beyond the range of the recommended correction factor for operating PWR's. On the other hand, the water density in these mock-up experiments is about 50% greater than under normal operating conditions, and so the higher soluble boron density can produce a larger reactivity discrepancy.

Because the leakage from these mock-up experiments is quite low, a change in group structure would have very little effect and so only a fine-mesh correction is needed. A finer mesh spacing, two

mesh spaces per pin cell side rather than one, was selected and the two-dimensional calculations for loads 1, 2, and 8 were re-run.

As Figures 6-4, 6-5, and 6-6 illustrate, this change produced a significantly better value for the multiplication factor for load 2 and left the multiplication factors for loads 1 and 8, which were already in good agreement with the experimental data, essentially unchanged. (The convention adopted in these Figures is that water holes are represented by an "X" and that BPR's are represented by a "+".) In load 1, no non-fuel locations are present and so no correction is necessary. In load 8, the BPR parameterization itself, which preserves the reaction rate predicted by EPRI-CELL by adjusting the PDQ thermal MND absorption cross section for the BPR, produces a BPR worth which is mesh independent.

Calculations also have been performed for loads 3 and 9, and the results are presented in Figures 6-7 and 6-8, respectively.

Once this mesh change was made in PDQ-7, the ARMP system produced excellent agreement with the measured data from all five loads. No additional modification of any of the ARMP procedures was needed, and it should be emphasized that this one change was necessitated by the high density of the moderator, relative to normal operating conditions. EPRI-CELL therefore has been shown to describe accurately the neutronic behavior of BPR's, even when they are as heavily loaded as the ones in these experiments.

1.026 1.026	1.025 1.025	1.022 1.022	1.018 1.018	1.013 1.013	1.005 1.005	.997 .996	.986 .986
	1.024 1.024	1.021 1.021	1.017 1.017	1.012 1.012	1.004 1.004	.996 .996	.985 .985
		1.019 1.019	1.015 1.015	1.009 1.009	1.002 1.002	.993 .993	.983 .983
			1.011 1.011	1.005 1.005	.998 .998	.989 .989	.979 .979
				1.000 1.000	.992 .991	.984 .984	.973 .973
					.985 .985	.976 .976	.966 .966
						.968 .968	.958 .957
							.947 .947

Relative Pin Power in Central Subassembly

	K_{EFF}	K_∞	M^2
EXPERIMENT	1.0007	-	-
ARMP, STANDARD	.9999	1.0182	35.64
ARMP, FINER MESH	.9998	1.0179	35.64

ARMP, STANDARD
ARMP, FINER MESH

FIGURE 6-4 Comparison of Results for Load 1

1.072 1.085 1.085	.993 1.010 1.004	.968 .985 .979	.992 .978 .973	.993 .978 .976	.948 .957 .955	.951 .934 .933
1.033 1.075 1.058	1.040 1.074 1.076	1.002 1.033 1.016	1.013 1.028 1.011	1.062 1.050 1.054	.993 .998 .986	.970 .940 .939
		1.080 1.087 1.088	1.082 1.087 1.089		1.035 1.036 1.043	.930 .947 .944
		1.056 1.096 1.069	1.108 1.122 1.117	1.096 1.102 1.099	.999 1.003 .992	.894 .939 .937
				1.073 1.056 1.060	.974 .959 .955	.942 .925 .925
				.982 .995 .983	.941 .936 .934	.940 .914 .916
					.939 .917 .918	.919 .905 .908
						.890 .896 .899

Relative Pin Power in Central Subassembly

	K_{EFF}	K_∞	M^2
EXPERIMENT	1.0007	-	-
ARMP, STANDARD	1.0052	1.0240	35.24
ARMP, FINER MESH	1.0018	1.0205	35.25

EXPERIMENT
ARMP, STANDARD
ARMP, FINER MESH

FIGURE 6-5 Comparison of Results for Load 2

1.102 1.114 1.120	.986 .998 .996	1.003 .990 .991	1.015 .996 .998	1.005 1.005 1.004	1.045 1.046 1.046	1.079 1.087 1.085
.995 .999 1.011	.907 .899 .890	.961 .924 .938	.943 .931 .945	.924 .914 .904	1.027 .993 1.003	1.061 1.077 1.078
		.864 .851 .844	.864 .855 .845		.961 .945 .932	1.044 1.070 1.072
		.878 .839 .860	.820 .816 .813	.896 .855 .851	1.007 .994 1.005	1.045 1.090 1.092
				.931 .926 .914	1.053 1.067 1.070	1.093 1.123 1.121
				1.028 1.021 1.030	1.095 1.115 1.116	1.147 1.153 1.150
					1.118 1.155 1.152	1.151 1.178 1.174
						1.158 1.196 1.191

Relative Pin Power in Central Subassembly

	K_{EFF}	K_∞	M^2
EXPERIMENT	1.0007	-	-
ARMP, STANDARD	.9993	1.0234	35.52
ARMP, FINER MESH	.9998	1.0234	35.54

EXPERIMENT
ARMP, STANDARD
ARMP, FINER MESH

FIGURE 6-6 Comparison of Results for Load 8

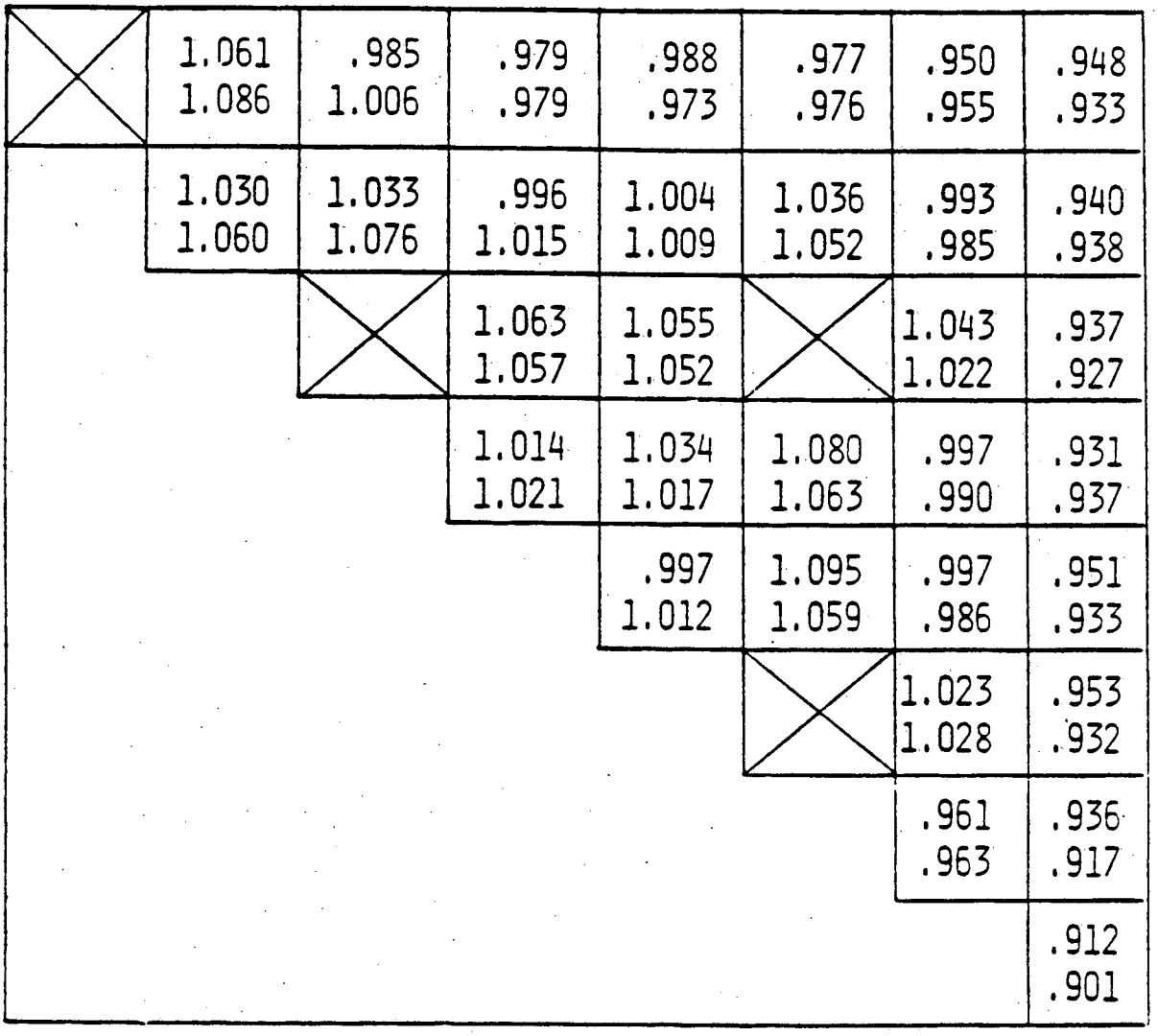

Relative Pin Power in Central Subassembly

	K_{EFF}	K_∞	M^2
EXPERIMENT	1.0007	-	-
ARMP, FINER MESH	1.0022	1.0209	35.25

EXPERIMENT
ARMP, FINER MESH

FIGURE 6-7 Comparison of Results for Load 3

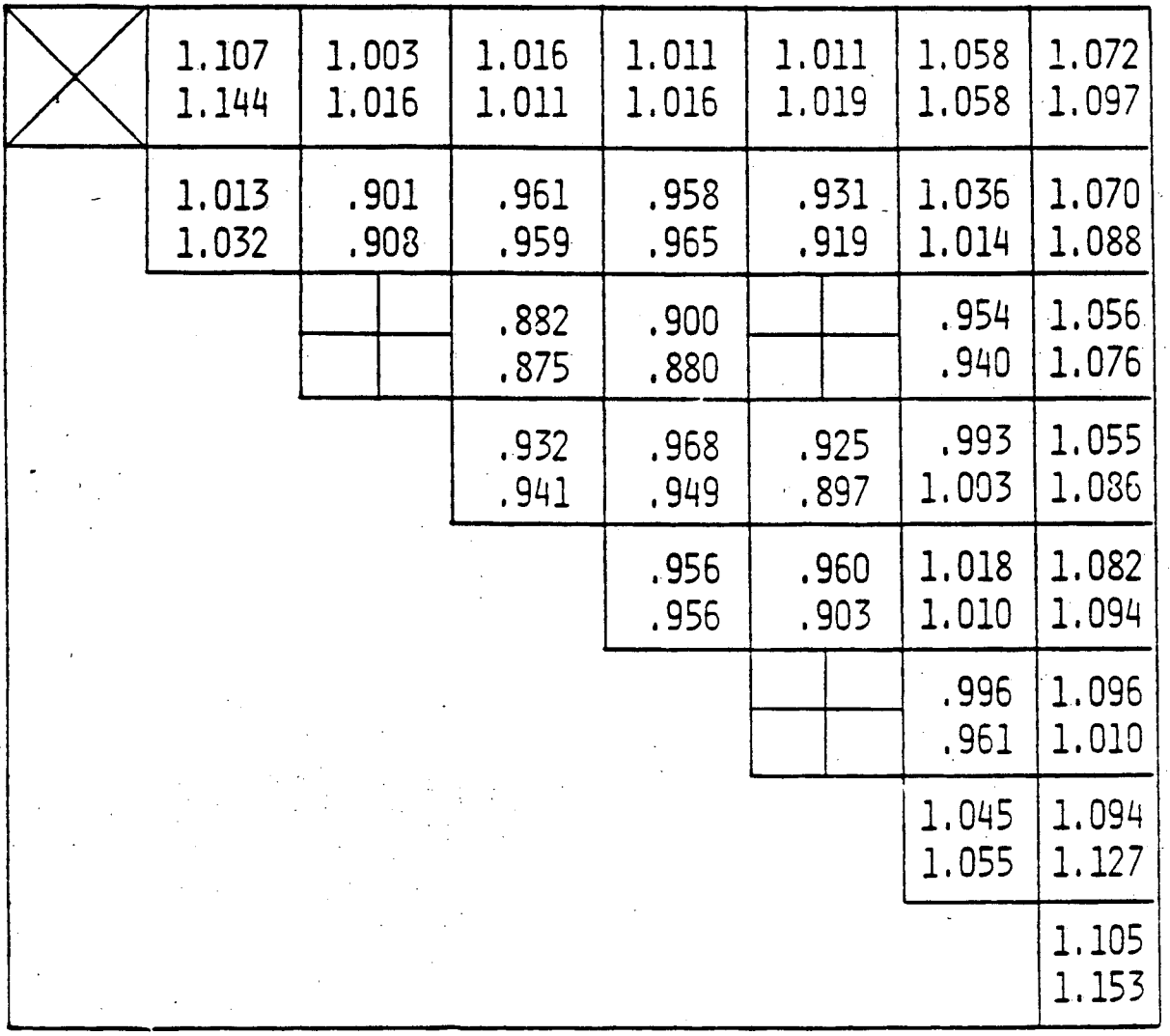

Relative Pin Power in Central Subassembly

	K_{EFF}	K_∞	M^2
EXPERIMENT	1.0007	-	-
ARMP, FINER MESH	.9997	1.0235	35.54

EXPERIMENT
ARMP, FINER MESH

FIGURE 6-8 Comparison of Results for Load 9

17. V.O. Uotinen, et al., "Lattices of Plutonium-Enriched Rods in Light Water--Part I: Experimental Results," Nucl. Tech., 15, 257 (1972).

18. H. Windsor and R. Goldstein, "Analysis of Lattices Containing Mixed-Oxide Fuel in Particulate Form," Trans. Am. Nucl. Soc., 15, 107 (1972).

19. Askew, et al., op cit.

20. Hellens, op cit.

21. M.N. Baldwin and M.E. Stern, "Physics Verification Program -- Part III, Task 4, Summary Report," BAW-3647-20 (1971).

Re Q. 12 Additional justification is required to support the conclusion that PDQ07 conservatively predicts maximum pin powers.

Re A. 12 Nuclear reactor cores are modeled in two dimensions at Duke Power Company using the PDQ07 code. A discrete pin geometry and two neutron energy group Mixed Number Density (MND) EPRI-CELL physics constants are used.

In the following figures, hot full power (HFP) PDQ07 and CASMO individual pin powers are presented from quarter-assembly calculations. These calculations were performed at beginning-of-life with no xenon; at this time pin power peaking is most severe. The enrichments used are typical of future reloads at Oconee. A variety of soluble boron concentrations and burnable poison (BP) weight percents (B_4C) were used. Also, water filled control rod guide tubes (CRGT) were used. All assemblies contained an instrument tube (IT). Table 1 identifies the five cases.

TABLE 1

Case	U-235 w/o	Absorber	PPM-Boron
1	3.08	1.0 w/o B_4C	500
2	3.08	1.0 w/o B_4C	1000
3	3.38	.2 w/o B_4C	1000
4	3.38	CRGT	1000
5	3.08	CRGT	0

In evaluating pin powers, the CASMO code solves the transport equation in two dimensions and seven neutron energy groups[1]. PDQ07 used only two energy groups in evaluating the diffusion equation. Therefore, the Duke PDQ07 model was tested not only by a higher order neutronics method, but also by more neutron energy groups.

In all five cases it is shown that PDQ07 predicts accurately and conservatively each assembly's maximum pin power. PDQ07 also predicted the same location of the maximum pin for each case as CASMO.

For pin powers equal to or greater than 1.000, pinwise powers usually agree within 1%. The CRGT cases, however, show PDQ07 to be up to 2% more conservative.

Therefore it is concluded from these comparisons, as well as those in NFS-1001 Supplement 2, that the two group MND PDQ07 accurately and conservatively predicts the maximum pin power within an assembly over a wide range of moderator and fuel temperatures, enrichments, soluble boron concentrations, and BP loadings.

1. These CASMO calculations were run using 69 energy groups in the microregion calculation.

FIGURE 1

QUARTER ASSEMBLY PINWISE POWERS - CASE 1

CODE	PDQØ7	CASMO	
K-INF	1.1419	1.1421	
U-235 w/o	3.08	3.08	
PPMB	500	500	
B-4-C w/o	1.0	1.0	

IT							
1.044 1.050	1.009 1.012	CASMO PDQØ7					
0.992 0.993	0.970 0.973	BP					
0.982 0.977	0.974 0.966	0.952 0.952	0.956 0.948				
0.981 0.975	0.973 0.965	0.952 0.952	0.946 0.947	BP			
0.986 0.980	0.967 0.968	BP	0.959 0.960	0.971 0.973	1.000 0.994		
1.003 1.000	0.997 0.992	0.981 0.986	0.997 0.994	1.010 1.007	1.024 1.022	1.041 1.043	
1.035 1.036	1.033 1.034	1.031 1.033	1.035 1.038	1.043 1.046	1.054 1.058	1.068 1.076	1.096 1.109

FIGURE 2

QUARTER ASSEMBLY PINWISE POWERS - CASE 2

CODE	PDQØ7	CASMO	
K-INF	1.0938	1.0930	
U-235 w/o	3.08	3.08	
PPMB	1000	1000	
B-4-C w/o	1.0	1.0	

IT							
1.043 1.049	1.009 1.012	CASMO PDQØ7					
0.992 0.993	0.971 0.974	BP					
0.983 0.978	0.975 0.967	0.953 0.954	0.958 0.950				
0.982 0.976	0.975 0.966	0.953 0.954	0.948 0.949	BP			
0.986 0.981	0.968 0.969	BP	0.960 0.961	0.972 0.974	1.000 0.994		
1.003 0.999	0.997 0.993	0.982 0.987	0.997 0.994	1.010 1.006	1.023 1.020	1.039 1.040	
1.034 1.035	1.032 1.033	1.030 1.032	1.034 1.036	1.042 1.045	1.052 1.056	1.065 1.073	1.092 1.105

FIGURE 3

QUARTER ASSEMBLY PINWISE POWERS - CASE 3

CODE	PDQØ7	CASMO	
K-INF	1.1891	1.1876	
U-235 w/o	3.38	3.38	
PPMB	1000	1000	
B-4-C w/o	0.2	0.2	

IT							
1.037 1.043	1.013 1.023	CASMO PDQØ7					
0.994 0.993	1.002 1.004	BP					
0.984 0.976	0.988 0.988	0.999 1.002	0.995 1.007				
0.982 0.972	0.986 0.986	0.999 1.003	1.003 1.014	BP			
0.984 0.975	0.995 0.994	BP	1.002 1.011	0.999 1.001	0.990 0.988		
0.988 0.980	0.992 0.991	1.001 1.002	0.994 0.996	0.991 0.986	0.990 0.983	0.995 0.989	
1.007 1.002	1.008 1.005	1.009 1.008	1.008 1.007	1.008 1.004	1.009 1.006	1.015 1.015	1.037 1.042

FIGURE 4

QUARTER ASSEMBLY PINWISE POWERS - CASE 4

CODE	PDQØ7	CASMO	
K-INF	1.2210	1.2170	
U-235 w/o	3.38	3.38	
PPMB	1000	1000	
B-4-C w/o	CRGT	CRGT	

IT							
1.024 1.028	1.011 1.029	CASMO PDQØ7					
0.990 0.989	1.028 1.031	CRGT					
0.980 0.971	0.996 1.006	1.041 1.050	1.030 1.063				
0.977 0.966	0.994 1.004	1.042 1.052	1.058 1.080	CRGT			
0.978 0.968	1.019 1.017	CRGT	1.046 1.062	1.028 1.030	0.983 0.985		
0.971 0.960	0.985 0.988	1.020 1.017	0.992 0.999	0.974 0.968	0.962 0.949	0.958 0.942	
0.980 0.967	0.983 0.975	0.988 0.983	0.984 0.977	0.977 0.966	0.972 0.959	0.974 0.961	0.993 0.984

FIGURE 5

QUARTER ASSEMBLY PINWISE POWERS - CASE 5

CODE	PDQØ7	CASMO	
K-INF	1.3272	1.3267	
U-235 w/o	3.08	3.08	
PPMB	0	0	
B-4-C w/o	CRGT	CRGT	

IT							
1.026 1.030	1.013 1.031	CASMO PDQØ7					
0.992 0.993	1.030 1.032	CRGT					
0.981 0.974	0.998 1.009	1.043 1.051	1.033 1.065				
0.978 0.969	0.996 1.006	1.044 1.053	1.060 1.080	CRGT			
0.979 0.970	1.019 1.016	CRGT	1.047 1.061	1.028 1.029	0.982 0.985		
0.971 0.960	0.985 0.988	1.020 1.016	0.992 0.999	0.974 0.968	0.960 0.948	0.956 0.941	
0.979 0.966	0.982 0.974	0.987 0.982	0.982 0.976	0.975 0.964	0.969 0.956	0.970 0.958	0.989 0.979